Monthly Notices
of the
ROYAL ASTRONOMICAL SOCIETY

Mon. Not. R. Astron. Soc. **417,** 3025–3034 (2011) doi:10.1111/j.1365-2966.2011.19459.x

Gamma-ray burst rate: high-redshift excess and its possible origins

Francisco J. Virgili,[1⋆] Bing Zhang,[1⋆] Kentaro Nagamine[1⋆] and Jun-Hwan Choi[2]

[1]*Department of Physics and Astronomy, University of Nevada Las Vegas, 4505 Maryland Parkway, Las Vegas, NV 89154, USA*
[2]*Department of Physics and Astronomy, University of Kentucky, 600 Rose Street, Lexington, KY 40506, USA*

Accepted 2011 July 18. Received 2011 July 15; in original form 2011 May 23

ABSTRACT

Prompted by various analyses of long (type II) gamma-ray burst (GRB) rates and their relationship to the cosmic star formation history, metallicity and luminosity function evolution, we systematically analyse these effects with a Monte Carlo code. We test various cosmic star formation history models including analytical and empirical models as well as those derived from cosmological simulations. We also explore expressions for metallicity enhancement of the GRB rate with redshift, as presented in the literature, and discuss improvements to these analytic expressions from the point of view of galactic evolution. These are also compared to cosmological simulations on metal enrichment. Additionally, we explore possible evolutionary effects of the GRB rate and luminosity function with redshift. The simulated results are tested with the observed *Swift* sample including the L, z and peak flux ($\log N$–$\log P$) distributions. The observational data imply that an increase in the GRB rate is necessary to account for the observations at high redshift, although the form of this enhancement is unclear. A rate increase due to lower metallicity at higher redshift may not be the singular cause and is subject to a variety of uncertainties. Alternatively, evolution of the GRB luminosity function break with redshift shows promise as a possible alternative.

Key words: methods: statistical – gamma-ray burst: general.

1 INTRODUCTION

Since firmly establishing the cosmological nature of type II (long-soft) gamma-ray bursts (GRBs) (Metzger et al. 1997; van Paragijs et al. 1997), there have been many predictions as to how early in cosmic history GRBs are created. Redshifts for GRBs have been detected more effectively since the 2004 launch of the *Swift* satellite (Gehrels et al. 2004) which has the advantage of providing prompt localizations. This, combined with the dedicated work of ground-based astronomers, has shown progress in pushing towards the theoretical detection limit of about a $z \sim 20$ (Abel, Bryan & Norman 2002; Bromm & Loeb 2002). Record-breaking bursts, such as GRB 050904 ($z = 6.3$; Cusumano et al. 2006; Frail et al. 2006; Haislip et al. 2006; Kawai et al. 2006), GRB 080913 ($z = 6.7$; Greiner et al. 2009) and GRB 090423 ($z = 8.2$; Salvaterra 2009b; Tanvir et al. 2009) demonstrate just how far these objects can be detected and warrant a discussion on how bursts that occur at such drastically different times in the evolution of the Universe may or may not differ.

It is believed that type II[1] GRBs are a product of the core collapse of massive stars, stemming from the evidence of an association of these GRBs with core-collapse supernovae (Hjorth et al. 2003; Stanek et al. 2003). These observations lead naturally to the expectation that the rate of these objects follow the cosmic star formation history (SFH; Wijers et al. 1998; Totani 1999; Blain & Natarajan 2000; Lamb & Reichart 2000; Porciani & Madau 2001). Various studies have shown that the rate of GRBs does not strictly follow the SFH but is actually enhanced by some mechanism at high z (Daigne, Rossi & Mochkovitch 2006; Guetta & Piran 2007; Le & Dermer 2007; Salvaterra & Chincarini 2007; Kistler et al. 2008, 2009; Li 2008; Salvaterra 2009a,b; Campisi, Li & Jakobsson 2010; Qin et al. 2010; Wanderman & Piran 2010), be it metallicity effects (Langer & Norman 2006; Li 2008), selection effects or an increase in luminosity.

In this analysis, we combine and expand various elements from these works to further analyse possible GRB rate enhancements with redshift and the underlying causes and forms of these evolutions using the available observational data together with a Monte Carlo code. We look into the underlying form of the cosmological SFH, including models derived from cosmological smoothed

⋆E-mail: virgilif@physics.unlv.edu (FJV); zhang@physics.unlv.edu (BZ); kn@physics.unlv.edu (KN)

[1] See Zhang et al. (2009) for a full discussion on the classification of GRBs and a full description of the distinction between type I and type II bursts.

particle hydrodynamic (SPH) simulations (Choi & Nagamine 2010), metallicity effects, rate evolution with redshift and evolution of the break luminosity of the GRB luminosity function.

In Section 2, we present and explain the details of the various simulations that were conducted, broken down by the form of the SFH or high-z enhancement (e.g. metallicity or evolution effect). Section 3 explains the method of testing for consistency. Section 4 details the results for the simulations in the same framework as Section 2, dedicating a section to each form of enhancement. We conclude with a summary and discussion in Section 5.

2 THEORY AND SIMULATIONS

One of the major goals of this and previous analyses is to constrain the *intrinsic* distribution of GRBs by utilizing the available *observed* data. We develop a Monte Carlo code that randomly creates a set of GRBs, defined by a luminosity and redshift pair from assumed luminosity and redshift distributions, and cycles them through a series of filters that act as a 'detection'. The set-up is similar to that of Virgili, Liang & Zhang (2009) but with various additions and improvements tailored to this specific problem. The set of generated bursts is then compared to the current observations of the luminosity, redshift and peak flux (i.e. $\log N$–$\log P$) distributions. The observed GRB rate follows the form

$$\frac{\mathrm{d}N}{\mathrm{d}t\,\mathrm{d}z\,\mathrm{d}L} = \frac{R_{\mathrm{GRB}}(z)}{1+z}\frac{\mathrm{d}V(z)}{\mathrm{d}z}\Phi(L), \tag{1}$$

where the $(1+z)$ factor accounts for the cosmological time dilation, $R_{\mathrm{GRB}}(z)$ is the GRB volume event rate (in units of $\mathrm{Gpc}^{-3}\,\mathrm{yr}^{-1}$) as a function of z, $\Phi(L)$ is the luminosity function and $\mathrm{d}V(z)/\mathrm{d}z$ the comoving volume element given by

$$\frac{\mathrm{d}V(z)}{\mathrm{d}z} = \frac{c}{H_0}\frac{4\pi D_L^2}{(1+z)^2[\Omega_{\mathrm{m}}(1+z)^3+\Omega_\Lambda]^{1/2}} \tag{2}$$

for a flat Λ cold dark matter (ΛCDM) universe. We assume $H_0 = 71\,\mathrm{km\,s^{-1}\,Mpc^{-1}}$, $\Omega_{\mathrm{m}} = 0.3$ and $\Omega_\Lambda = 0.7$ throughout.

Equation (1) has two unknowns to be explored, the luminosity function term being the more straightforward. Numerous analyses have explored this topic in various contexts (Schmit 2001; Lloyd-Ronning, Fryer & Ramirez-Ruiz 2002; Norris 2002; Stern, Atteia & Hurley 2002; Lloyd-Ronning, Dai & Zhang 2004; Coward 2005; Guetta, Piran & Waxman 2005; Cobb et al. 2006; Daigne, Rossi & Mochkovitch 2006; Pian et al. 2006; Soderberg et al. 2006; Chapman et al. 2007; Liang et al. 2007; Dai 2009; Virgili et al. 2009; Qin et al. 2010; Wanderman & Piran 2010). We adopt the generally accepted broken power-law model:

$$\Phi(L) = \Phi_0\left[\left(\frac{L}{L_{\mathrm{b}}}\right)^{\alpha_1} + \left(\frac{L}{L_{\mathrm{b}}}\right)^{\alpha_2}\right]^{-1}, \tag{3}$$

where α_1 and α_2 are the power-law indices, L_{b} the break luminosity and Φ_0 a normalization constant. We consider solely 'classical' high-luminosity GRBs, ignoring local low-luminosity events and their contribution to the luminosity function (Coward 2005; Le & Dermer 2007; Liang et al. 2007; Virgili et al. 2009) in order to have as unbiased a sample as possible.

The GRB rate, $R_{\mathrm{GRB}}(z)$, is the main focus of this analysis as it is a convolution of the SFH, metallicity and evolution effects. Next, we present the specifics of each SFH model and enhancement.

2.1 Cosmic star formation history

The cosmic SFH is the basis for the rate distribution from which we choose our redshift values for the simulated GRBs. Many forms are available in the literature, but it is generally believed that the SFH increases rapidly to about $z \sim 1$–2, then slowly falls off towards higher redshift, and we use a variety of forms presented in the literature. Hopkins & Beacom (2006, hereinafter HB) have compiled a widely accepted model fit from numerous multiband observations (see HB, and references therein). Bromm & Loeb (2006, hereinafter BL) present a comprehensive model for the SFH based on a flat ΛCDM cosmological model with the added contribution of Population III stars at high redshift. As a control, we also include the SF2 model of Porciani & Madau (2001, hereinafter PM; see Fig. 1) based on estimates from ultraviolet (UV) continuum and Hα emission. A list of SFH models used is summarized in Table 1.

In addition, we utilize a model derived from cosmological SPH simulations of Choi & Nagamine (2010, hereinafter CN). They developed a modified version of GADGET-3 code (originally described in Springel 2005), including radiative cooling by H, He and metals

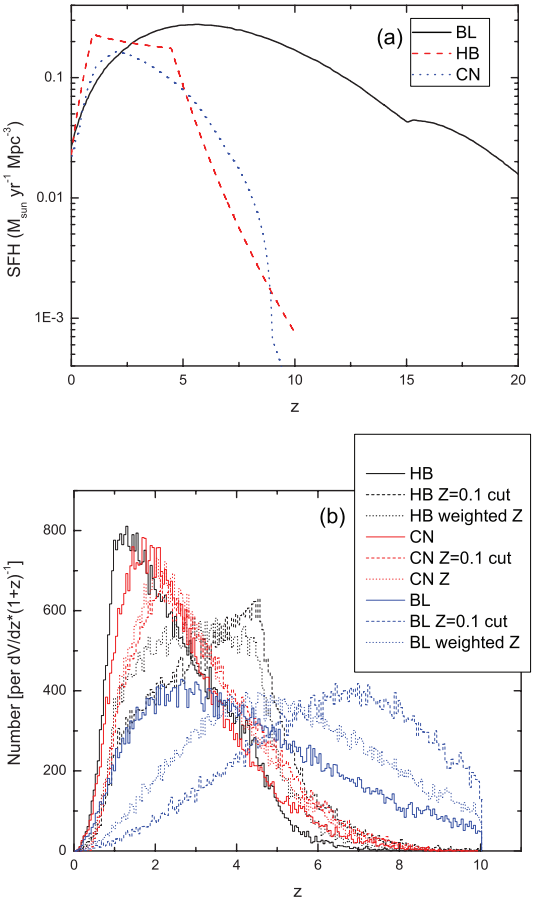

Figure 1. Panel (a): SFH models utilized in the analysis. Panel (b): simulated relative number of GRBs per unit comoving volume $\times\ (1+z)^{-1}$ for different models. This panel shows the output from the code without a threshold, so as to check the underlying distribution and see the relative affects of the metallicity relations on the base SFH.

Table 1. Summary of SFH models.

SFH Model	Reference
PM	Porciani & Madau (2001)
HB	Hopkins & Beacom (2006)
BL	Bromm & Loeb (2006)
CN	Choi & Nagamine (2010)

(Choi & Nagamine 2009), heating by a uniform UV background of a modified Haardt & Madau (1996) spectrum (Katz, Weinberg & Hernquist 1996; Davé et al. 1999), a subresolution model of multiphase interstellar medium (Springel & Hernquist 2003), the 'Pressure' SF model (CN; Schaye et al. 2010) and the 'multicomponent variable velocity' (MVV) galactic wind model (Choi & Nagamine 2011a). They have shown that the metal line cooling enhances SF across all redshifts by about 10–30 per cent (Choi & Nagamine 2009) and that the Pressure SF model suppresses SF at high redshift due to a higher threshold density for SF (CN) with respect to the earlier model by Springel & Hernquist (2003). Choi & Nagamine (2011a) also showed that the MVV wind model, which is based on both momentum- and energy-driven galactic winds, makes the faint-end slope of the galaxy stellar mass function (GSMF) slightly shallower compared to the constant velocity galactic wind model of Springel & Hernquist (2003). The adopted cosmological parameters are consistent with the *Wilkinson Microwave Anisotropy Probe* (*WMAP*) best-fitting values (Komatsu et al. 2011): $\Omega_{\rm m} = 0.26$, $\Omega_\Lambda = 0.74$, $\Omega_{\rm b} = 0.044$, $h = 0.72$, $n_s = 0.96$ and $\sigma_8 = 0.80$. These values are only slightly different from those presented in Section 2. The results from three simulations with box sizes of comoving 10, 34 and 100 h^{-1} Mpc were combined to obtain a full SFH, including galaxy stellar masses above 10^7 $M_\odot$ (Choi & Nagamine 2011b).

2.2 Metallicity

One popular explanation for possible enhancements of the GRB rate is the effect due to decreasing metallicity with redshift (Fynbo et al. 2003; Chen et al. 2005; Conselice et al. 2005; Gorosabel et al. 2005; Starling et al. 2005; Langer & Norman 2006; Li 2008; Butler et al. 2010; Campisi et al. 2010; Qin et al. 2010). If GRBs occur more frequently in low-metallicity environments, then this could be a possible mechanism for enhancing the GRB rate at high redshift. Langer & Norman (2006, hereinafter LN) proposed an analytical form for the mass density fraction in galaxies with a mass less than M, based on the GSMF. This mass is then related to the amount of metals via the galaxy mass–metallicity relation (Tremonti et al. 2004; Savaglio et al. 2005), giving

$$\Psi\left(\frac{Z}{Z_\odot}\right) = \frac{\hat{\Gamma}[\alpha_{\rm G}+2, (Z/Z_\odot)^\beta 10^{0.15\beta z}]}{\Gamma[\alpha_{\rm G}+2]}, \quad (4)$$

where $\hat{\Gamma}$ and Γ are the incomplete and complete γ functions, β the power index of the galaxy mass–metallicity relation and $\alpha_{\rm G}$ the faint-end slope of the GSMF. To begin, we utilize this relation with constant parameters from the literature [$\alpha_{\rm G} = -1.16$, $\beta = -2$, $\epsilon = (Z/Z_\odot) = 0.1$; LN; Li 2008] and then build upon it to formulate a weighted version to account for the more realistic case of variations in metallicity from $\epsilon = 0.1$–0.4 (Fig. 2). This function also contains many assumptions about the underlying mass distribution and mass–metallicity relation which we will expand on in Section 4.4.

The cosmological simulations derive SF rates for populations of stars from various metallicities without the need of an external expression. At every time-step, star particles are created in high-density regions that exceed the threshold density according to the SF law matched to the locally observed Kennicutt (1998) law. Once a star particle is created, instantaneous recycling is assumed, and the metals are ejected with a yield of $Y = 0.02$ and distributed to the nearby environment by a galactic wind. Niino et al. (2011) have used similar simulations to examine the metallicity of GRB host galaxies, and found good agreement with observations. See Fig. 2 for a comparison of equation (4) and the result from cosmological simulations.

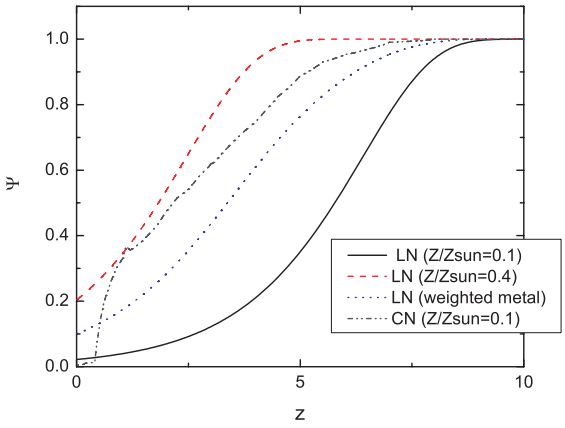

Figure 2. Fractional stellar mass density contained in galaxies with metallicities below $Z/Z_\odot$ (equation 4) from LN, including different metal cuts ($Z/Z_\odot = 0.1, 0.4$) and modifications from weighting. The expression derived from the SFH of CN with a metal cut of 0.1 is included for comparison.

2.3 Rate evolution

Motivated by the literature (e.g. Kistler et al. 2008, 2009; Qin et al. 2010) we include a discussion on an increase in the GRB rate with redshift as $(1+z)^\delta$. This is not to be confused with the evolution of the break luminosity of the luminosity function, which has the same functional form (see Section 2.4). The latter has a more physical meaning (e.g. GRBs becoming brighter with increased redshift), whereas the former is more of a general statement of the GRB rate, increasing in this fashion due to an unspecified process. The former may be related to an evolving stellar initial mass function (IMF) with redshift that causes a shift to a top-heavy stellar IMF (Wang & Dai 2011). These simulations assume $R_{\rm GRB} \propto {\rm SFH} \times (1+z)^\delta$ with a non-evolving luminosity function. The results of these simulations are presented in Section 4.5.

2.4 $L_{\rm b}$ evolution

The last form of enhancement of the GRB rate is evolution of the break of luminosity function, $L_{\rm b}$, with redshift. We take a similar functional form to the rate evolution, assuming that the luminosity function break evolves as $(1+z)^\gamma$. This increase manifests itself as an increase of bright bursts at higher redshifts, which increases their detection rate. Unlike the previous section, these simulations assume that $R_{\rm GRB}$ is proportional to the SFH and that the luminosity function break, $L_{\rm b}$, evolves as $(1+z)^\gamma$. The results of these simulations are presented in Section 4.6

2.5 Threshold and other details

Once a luminosity and redshift pair is chosen according to the distributions discussed above, it is necessary to adopt a threshold condition that mimics the detector in question. We adopt the threshold condition based on the probability of triggering *Swift* derived by Qin et al. (2010):

$$\eta_t = \begin{cases} 5.0P^{3.85}, & P < 0.45 \\ 0.67(1.0 - 0.40/P)^{0.52}, & P \geq 0.45 \end{cases} \quad (5)$$

where P is the photon flux of the burst in the 15–150 keV band. This equation is based on the similarities between the BATSE and *Swift* photon flux samples. By comparing the relative number of bursts, both triggered and untriggered, that occur in a particular photon flux

bin to the total number of bursts, it is possible to obtain a probability for triggering that instrument. Qin et al. (2010) were able to fit the distribution to derive equation (5). When comparing different detectors, it is necessary to have a normalized value for P, and Qin et al. found that the normalization for both detectors is similar, so one expression is a good approximation for both detectors. For comparisons with the observed redshift and luminosity samples, we include an additional probability for the detection of a redshift since not all bursts have redshifts. Similarly, a probability of assigning a redshift is found by looking at the distribution of bursts with redshift versus the total number of bursts per redshift bin. Qin et al. (2010) did not find a large distinction between these two samples but parametrized the probability as

$$\eta_z = 0.26 + 0.032\,\mathrm{e}^{1.61\log P}. \tag{6}$$

Both expressions and the $\log N$–$\log P$ analysis depend on the calculation of the photon flux. The *energy* flux is calculated directly from $F_{\rm peak} = L/4\pi D_L^2(z)k$, where $D_L(z)$ is the luminosity distance at a given redshift and k is the k-correction,

$$k = \frac{\int_{1/(1+z)}^{10^4/(1+z)} EN(E)\,\mathrm{d}E}{\int_{e_1}^{e_2} EN(E)\,\mathrm{d}E}, \tag{7}$$

which corrects the flux from the bolometric 1–10^4 keV band into the observed band (e_1, e_2). In equation (7), $N(E)$ is the photon spectrum of the GRB, which we assume to be a Band function (Band et al. 1993). The Band function is a smoothly joined power-law function that has pre- and post-break slopes α and β around a break energy E_0. The peak of the νF_ν spectrum, $E_{\rm peak}$, is related to this energy by $E_{\rm peak} = (2 + \alpha)E_0$. Since the peak energy of bursts changes with the energy of the burst (i.e. the Amati relation; Amati et al. 2002; Liang & Dai 2004), we utilize the relation derived by Liang & Dai (2004) to assign values for the simulated $E_{\rm peak}$:

$$E_{\rm peak}/200\,\mathrm{keV} = C^{-1}(L/10^{52}\,\mathrm{erg\,s^{-1}})^{1/2}, \tag{8}$$

where C is a random uniform deviate between [0.1,1] and L the luminosity. We also randomly sample α and β uniformly between $-0.83 < \alpha < -1.2$ and $-2.1 < \beta < -2.5$, which roughly correspond to the observed limits of these values. From these spectral parameters and peak energy flux, F, we then calculate the peak photon flux in the detector energy band (e_1, e_2) via

$$P = \frac{F\int_{e_1}^{e_2} N(E)\,\mathrm{d}E}{\int_{e_1}^{e_2} EN(E)\,\mathrm{d}E}. \tag{9}$$

3 TESTING FOR CONSISTENCY

Once we have a set of simulated bursts that are 'detected' and follow the GRB rate and luminosity function described above, it is necessary to test the consistency with the observed data. Our sample consists of 166 *Swift* and *HETE* era GRBs with known redshift through 2009 September. We remove the type I GRBs (see Zhang et al. 2009; Kann et al. 2011; Virgili et al. 2011), outlying low-luminosity bursts (GRB 980425 and GRB 060218) and any bursts with disputed or non-secure redshifts. This assumes that the observed redshift sample is the true intrinsic sample, although the detection of redshifts depends on a variety of observational factors and potential biases (Fiore et al. 2007; Jakobsson et al. 2011). In order to calculate the bolometric peak luminosity, it is necessary to have the energy or photon flux as well as the spectral information for the k-correction. Most *Swift* bursts are fitted by a simple power-law spectrum due to small bandpass of the *Swift* detector (Sakamoto et al. 2007). We instead assume all bursts to have a Band function spectrum (Band et al. 1993) utilizing the observed pre-break slope and assuming the typical value of 2.5 for the post-break slope, as assuming a simple power law extending to high energies will inevitably overestimate the high-energy contribution to the flux. This assumption is validated by observations of GRBs observed jointly with *Fermi* Large Area Telescope (LAT) and Gamma-ray Burst Monitor (GBM), where a Band function spectrum is seen over many orders of magnitude and extending to high energies (Abdo et al. 2009; Zhang et al. 2011). $E_{\rm peak}$ is used from the literature unless absent, in which case the value from catalogue of Butler et al. (2010) is used.

Next, the simulated set of 175 simulated bursts is compared to the observational sample with the k-sample Anderson–Darling (AD) test for consistency between two distributions (Scholz & Stephens 1987), giving the first three constraints (L alone, z alone, L–z together) to our models. Each criterion gives a contour showing the consistency with the observed sample in the $(\alpha_1, L_{\rm b})$ plane (see Fig. 4a shown later), with α_2 a constant of 2.2 or 2.5. We test both values of α_2, and results indicate which slope was used. Results are generally insensitive to the choice of α_2, and we take values quoted in the literature (Liang et al. 2007; Virgili et al. 2009; Qin et al. 2010).

The two $\log N$–$\log P$ tests are also conducted with the AD test and compares the simulations to the *Compton Gamma-ray Observatory* (*CGRO*)/BATSE and *Swift* photon flux samples. In order to have the most unbiased and complete sample from each, they are truncated at 0.4 [50–300 keV] and 1 photon $\mathrm{cm^{-2}\,s^{-1}}$ [15–150 keV], respectively (see Laredo & Waserman 1998; Band 2006) and compared to the 1143 BATSE and 380 triggered *Swift* bursts. A summary of various models and statistical results are presented in Tables 2–4.

4 RESULTS

4.1 GRB rate $\propto$ SFH

Clearly the simplest scenario possible for the GRB rate, this set of simulations showed little consistency with the current observations. Out of the four possible SFH models (PM; HB; BL; CN), only the BL model showed consistency with the observations (Table 2). The luminosity function is generally constrained to be shallow, with pre-break slopes generally shallower than ~ -0.2, and shows that there is the need for some form of increase of the rate compared to other SFH models at higher redshifts. Determining the form and possible cause(s) of this increase in GRB rate is a major goal of this analysis. This model, however, is based on the theory that the rate enhancements produced at high z are attributed to the contribution of Population III stars that were developing in the early Universe $z \sim 15$. To date, observations have not shown that GRBs arise from Population III stars (Salvaterra 2009b; Tanvir et al. 2009), and we caution drawing an association based solely on the form of this SFH.

4.2 GRB rate $\propto$ SFH+Metallicity cut-off

The next step, as detailed above, is to consider the addition of a term that in some manner accounts for an increase in the GRB rate in lower metallicity environments. A key component believed to aid in the creation of type II GRB is a fast-rotating core of the progenitor star. Low metallicities may help in reducing the mass-loss rate and retain sufficient angular momentum to keep the star rotating quickly and assist in the formation of the GRB jet. First, we consider the

Table 2. SFH models and test statistics for a variety of simulations, including a metallicity cut of $Z/Z_{\odot} = 0.1$. If consistency is found with the L and z samples, indicated by a 'Y' in the second column, then the luminosity function (LF) parameters are listed with the outcomes of the $\log N$–$\log P$ analysis. Later models include the addition of metallicity in the form of the expression from LN, but with a $Z/Z_{\odot} = 0.1$ cut as well as the weighted expression. An 'N' in the significance column indicates that test fails beyond a 3σ level. A similar analysis, with similar results, was conducted for models with the luminosity function post-break slope $\alpha_2 = 2.5$. Columns 8 and 10 indicate the significance level for the BATSE ad *Swift* $\log N$–$\log P$ tests, respectively.

Model	L–z? Y/N	LF parameters (α_1, L_b, α_2)	z Stat, P value	L Stat, P value	Significance z/L	BATSE LNLP T stat, P value	Sig	*Swift* LNLP T stat, P value	Sig
GRB rate $\propto$ *SFH* $\alpha_2 = 2.2$									
HB	N	–	–	–	–	–	–	–	–
BL	Y	(0.01, 500, 2.2)	−0.637 27, 0.519 55	1.496 13, 0.078 69	$1\sigma/2\sigma$	0.921 94, 0.139 39	2σ	0.188 29, 0.282 73	2σ
	Y	(0.11, 600, 2.2)	1.166 38, 0.109 32	−0.340 06, 0.429 21	$2\sigma/1\sigma$	0.425 51, 0.225 37	2σ	0.978 59, 0.131 78	2σ
	Y	(0.2, 900, 2.2)	1.4281, 0.0842	−0.336 04, 0.428	$2\sigma/1\sigma$	3.720 49, 0.010 36	3σ	0.958 44, 0.134 44	2σ
CN	N	–	–	–	–	–	–	–	–
PM	N	–	–	–	–	–	–	–	–
GRB rate $\propto$ *SFH + Metallicity* $\alpha_2 = 2.2$									
HB+Li	N	–	–	–	–	–	–	–	–
BL+Li	N	–	–	–	–	–	–	–	–
CN 0.1 cut	N	–	–	–	–	–	–	–	–
HB+Li weighted	Y	(0.11, 600, 2.2)	0.881 34, 0.145 09	−0.089 52, 0.356 32	$2\sigma/1\sigma$	1.973, 0.049 21	3σ	0.179 74, 0.284 85	2σ
	Y	(0.19, 1000, 2.2)	0.248 96, 0.267 93	−0.801 14, 0.5692	$2\sigma/1\sigma$	0.3929, 0.232 35	2σ	0.485 79, 0.212 93	2σ
	Y	(0.15, 800, 2.2)	0.297 43, 0.256 47	−0.4227, 0.454 11	$2\sigma/1\sigma$	1.073 91, 0.119 87	2σ	−0.219 68, 0.393 59	1σ
BL+Li weighted	N	–	–	–	–	–	–	–	–
CN weighted	N	–	–	–	–	–	–	–	–

Table 3. SFH models and test statistics for models with evolving GSMF faint-end slope, α_G, in the metallicity equation of LN. If consistency is found with the L and z samples, indicated by a 'Y' in the second column, then the LF parameters are listed with the outcomes of the $\log N$–$\log P$ analysis. 'sml scatter' and 'lrg scatter' indicate the amount of scatter in the weighting of the metallicity relation, 0.1 and 0.2, respectively. 'central values' and 'upper limits' indicate what set of α_G values were used in the analysis, those corresponding to the data point value or the upper limits in Fig. 3(a). An 'N' in the significance column indicates that test fails beyond a 3σ level. All models assume the post-break slope of the luminosity function $\alpha_2 = 2.2$. Columns 8 and 10 indicate the significance level for the BATSE ad *Swift* $\log N$–$\log P$ tests, respectively.

Model	L–z? Y/N	LF parameters (α_1, L_b, α_2)	z Stat, P value	L Stat, P value	Significance z/L	BATSE LNLP T stat, P value	Sig	*Swift* LNLP T stat, P value	Sig
Models including α_G *evolution (data point values)*									
HB+Li+α_G evol	Y	(0.1, 800, 2.2)	2.851 89, 0.021 64	−0.611 41, 0.511 65	$3\sigma/1\sigma$	0.211 95, 0.2769	2σ	0.843 84, 0.150 56	2σ
HB+Li+α_G evol+weighting (sml scatter)	N	–	–	–	–	–	–	–	–
HB+Li+α_G evol+weighting (lrg scatter)	N	–	–	–	–	–	–	–	–
BL+Li+α_G evol	Y	(0.41, 900, 2.2)	0.191 57, 0.281 91	−0.379 04, 0.440 92	$2\sigma/1\sigma$	18.105 81, 0	N	1.499 81, 0.0784	2σ
BL+Li+α_G evol+weighting (sml scatter)	Y	(0.39, 800, 2.2)	1.6878, 0.065 07	−0.073 09, 0.351 73	$2\sigma/1\sigma$	35.234 25, 0	N	2.739 04, 0.023 95	3σ
BL+Li+α_G evol+weighting (lrg scatter)	Y	(0.39, 900, 2.2)	0.841 06, 0.150 97	−0.702 35, 0.539 37	$2\sigma/1\sigma$			0.742 28, 0.166 33	2σ
Models including α_G *evolution (upper limit)*									
HB+Li+α_G evol	Y	(0.05, 600, 2.2)	2.5823, 0.027 63	−0.175 85, 0.380 88	$2\sigma/1\sigma$	4.422 84, 0.005 85	3σ	0.043 75, 0.319 89	2σ
HB+Li+α_G evol+weighting (sml scatter)	N	–	–	–	–	–	–	–	–
HB+Li+α_G evol+weighting (lrg scatter)	N	–	–	–	–	–	–	–	–
BL+LN+α_G evol	N	–	–	–	–	–	–	–	–
BL+LN+α_G evol+weighting (sml scatter)	N	–	–	–	–	–	–	–	–
BL+LN+α_G evol+weighting (lrg scatter)	N	–	–	–	–	–	–	–	–

formalism of Langer & Norman (2006; see also Li 2008; Qin et al. 2010) as detailed in equation (4), for all models with the exception of CN, as they form stars self-consistently according to metal line cooling rates in the simulation. The derivation is straightforward and clear in Langer & Norman (2006); however, there are various assumptions in this model that need to be addressed. The basis for this relation is the GSMF, which is assumed to be a Schechter function (i.e. a power law with exponential cut-off; equation (1) in LN, and references therein). The amount of galaxy stellar mass within a mass M is then related to the amount of metals by the

Table 4. SFH models and test statistics for models with rate evolution proportional to $(1+z)^{\delta}$ and luminosity function break luminosity ($L_{\rm b}$) evolution as $(1+z)^{\gamma}$. For the former, we show the results for $\delta = 0.2$ as an example. The results for $\delta = 0.5$ and 0.8 are similar, showing inconsistency with the BATSE and many *Swift* log N–log P constraints. An 'N' in the significance column indicates that test fails beyond a 3σ level. Columns 8 and 10 indicate the significance level for the BATSE and *Swift* log N–log P tests, respectively.

Model	L–z? Y/N	LF parameters (α_1, $L_{\rm b}$, α_2)	z Stat, P value	L Stat, P value	Significance z/L	BATSE LNLP T stat, P value	Sig	*Swift* LNLP T stat, P value	Sig
Rate evolution with z									
GRB rate $\propto$ *SFH*$*(1+z)^{\delta}$									
$\delta = 0.2$									
BL	Y	(0.05, 400)	–	–	–	–	N	–	2σ
	Y	(0.18, 500)	–	–	–	–	N	–	2σ
	Y	(0.24, 800)	–	–	–	–	N	–	2σ
	Y	(0.29, 800)	–	–	–	–	N	–	2σ
HB	N	–	–	–	–	–	–	–	–
CN	N	–	–	–	–	–	–	–	–
PM	N	–	–	–	–	–	–	–	–
BL+Li	N	–	–	–	–	–	–	–	–
HB+Li	N	–	–	–	–	–	–	–	–
CN 0.1 cut	N	–	–	–	–	–	–	–	–
BL+LN weighted	Y	(0.54, 900, 2.2)	–	–	–	–	N	–	N
	Y	(0.46, 700, 2.2)	–	–	–	–	N	–	N
	Y	(0.4, 500, 2.2)	–	–	–	–	N	–	N
	Y	(0.24, 400, 2.2)	–	–	–	–	N	–	N
HB+LN weighted	Y	(0.54, 900, 2.2)	–	–	–	–	N	–	3σ
	Y	(0.54, 900, 2.2)	–	–	–	–	N	–	3σ
CN weighted	N	–	–	–	–	–	–	–	–
LF break evolution									
$L_{\rm b} \propto L_{\rm b}*(1+z)^{\gamma}$									
$\gamma = 1.0$									
HB	Y	(0.15, 500)	2.773 68, 0.023 21	−0.378 16, 0.440 65	3σ/ 1σ	8.981 13, 0.000 15	N	2.046 78, 0.045 82	3σ
CN	Y	(0.05, 300)	0.9696, 0.132 96	−0.662 68, 0.5273	2σ/ 1σ	0.132 96, 0.296 64	2σ	−0.006 99, 0.333 53	1σ
	Y	(0.09, 400)	1.332 65, 0.0926	−0.499 87, 0.477 58	2σ/ 1σ	2.869 31, 0.0213	3σ	0.646 14, 0.182 62	2σ
	Y	(0.23, 500)	2.995 02, 0.019 06	0.240 22, 0.270 03	3σ/ 1σ	−0.599 66, 0.508 07	1σ	0.504 19, 0.209 24	2σ
	Y	(0.23, 800)	1.949 44, 0.050 35	1.819 83, 0.057 14	2σ/ 2σ	9.084 64, 1.40E−04	N	1.496 38, 0.078 67	2σ
	Y	(0.16, 600)	0.972 82, 0.132 53	−0.037 63, 0.341 91	2σ/ 1σ	6.355 83, 0.001 24	N	2.123 31, 0.042 56	3σ
$\gamma = 1.1$									
CN	Y	(0.13, 300)	1.1944, 0.1063	−0.601 68, 0.508 68	2σ/ 1σ	−0.109 03, 0.361 81	1σ	0.318 54, 0.251 58	2σ
$\gamma = 1.2$									
HB	Y	(0.12, 300)	3.431 85, 0.013 11	−0.861 34, 0.587 14	3σ/ 1σ	5.134 02, 0.003 31	3σ	0.901 69, 0.142 21	2σ
CN	Y	(0.23, 500)	1.634 19, 0.068 61	1.256 77, 0.099 89	2σ/ 2σ	3.683 55, 0.010 67	3σ	0.327 01, 0.246 97	2σ
	Y	(0.08, 200)	1.662 39, 0.066 72	−1.024 53, 0.634 52	2σ/ 1σ	−0.588 47, 0.504 65	1σ	1.269 17, 0.098 66	2σ
$\gamma = 1.3$									
CN	Y	(0.12, 200)	1.337 72, 0.092 14	−0.334 12, 0.427 43	2σ/ 1σ	−0.658 32, 0.525 97	1σ	0.1113, 0.3022	2σ
$\gamma = 1.4$									
CN	Y	(0.17, 300)	1.613 82, 0.070 01	0.829 04, 0.152 77	2σ/ 2σ	1.655 49, 0.067 18	2σ	1.002 56, 0.128 68	2σ
$\gamma = 1.5$									
CN	Y	(0.23, 200)	1.738 98, 0.061 87	0.605 85, 0.189 86	2σ/ 2σ	−0.823 08, 0.575 76	1σ	0.144 52, 0.2937	2σ

mass–metallicity relation, of the form $M/M^* = K(Z/Z_{\odot})^{\beta}$, where K and β are constants that are constrained by observation (Tremonti et al. 2004; Savaglio et al. 2005) and M^* is the characteristic mass of the GSMF. Previous studies do not address the scatter and/or evolution with redshift of the GSMF faint-end slope $\alpha_{\rm G}$, and assume that the average cosmic metallicity of the Universe decreases as $\mathrm{d}[Z]/\mathrm{d}z = -0.15$ dex. The normalization of the mass–metallicity relation changes with redshift, and for a particular metal cut $\epsilon = (Z/Z_{\odot})$, the mass fraction of metals also changes. This effect is reflected in the $10^{0.15\beta z}$ term of equation (4). Changes to this term are not examined explicitly.

Using this relation with the parameters assumed in Langer & Norman (2006) ($\alpha_{\rm G} = -1.16, \beta = 2$) and a cut-off metallicity for production of GRBs of $\epsilon = Z/Z_{\odot} = 0.1$, we find that no models agree with the L and z constraints to the 2σ level. The cosmological simulation results are similar and show that a strict metal cut at $Z/Z_{\odot} = 0.1$ is insufficient to explain the observations.

4.3 GRB rate $\propto$ SFH+Weighted metallicity

Building upon the previous section, we introduce a weighting to the metallicity cut in order to broaden the scope of equation (4). It is more realistic to consider a range of metallicities in which GRBs can occur, especially since GRBs have been observed in environments with metallicity greater than 0.1 (Holland et al. 2010; Levesque et al. 2010). Instead of taking the value of the relation from Langer & Norman (2006) for a particular value of ϵ, we instead weight the effect of different metallicities, ranging from $Z/Z_{\odot} = 0.1$ to 0.4,

for a particular redshift. We have utilized a Gaussian (with $\sigma = 0.1$ or 0.2) to weight the contributions of metals so that there is an exponential (rather than sharp) cut above the critical metallicity. The contributions from various metallicities are then added with proper weighting to produce an 'effective' Ψ (equation 4). This approach yields an intermediate solution between strict metal cuts of 0.1 and 0.4 (Fig. 2). A similar approach is taken for the CN model utilizing the SFR for different metal cuts provided from the simulation instead of applying equation (4).

Using this formulation, we re-run the previous SFH models and find that the HB model is the only model that can pass all of the observational tests, including the $\log N$–$\log P$, giving luminosity function parameters in the range of (α_1, $\alpha_2 = 2.2$, L_b) = (0.11–0.19, 2.2, 6–10 $\times$ 10^{52} erg s^{-1}) (Fig. 4; Table 2). The BL model, with its intrinsically large rate at high z, overproduces bursts at high z when metallicity is added.

4.4 More on the metallicity approximation

Up to this point, the analysis does not directly compare how the assumed metallicity relation (equation 4) affects the GRB rate compared to the cosmological simulations. This is an important and related topic, since the models that use the LN expression show consistency with the observations of type II GRBs, while the more rigorous and complete method of CN to calculate the metallicity shows no consistency. The differences, we come to find, are non-negligible. Why would the HB and CN models, whose total SF rates are quite similar, differ so largely when their respective metal cuts are applied (Fig. 1b)? The relation from Langer & Norman (2006) is an approximation to a very complex problem in galaxy evolution. The cosmological simulations by Choi & Nagamine (2010) address a variety of effects that contribute to the metal distribution (such as mixing due to galactic outflow and tidal disruption), and calculate the SF rate self-consistently according to varying metal line cooling rate. From those values, a realistic view of how the total rate is affected by the reduction in metallicity can be calculated, which is just what equation (4) shows: the net effect to the total SF rate by a metallicity cut at $Z/Z_\odot$. The curves for various values of $Z/Z_\odot$ are shown together with the equivalent expression from the CN (Figs 2 and 3).

Since these expressions are so different, we attempt to look at the structure of the Langer & Norman (2006) expression and see if any part(s) can be improved to create a more realistic view of how metallicity affects the rate of GRBs. The first major assumption in equation (4) is the constant value of the GSMF slope, α_G, which is observed to be steepening with z (Bouwens et al. 2010, and references therein), suggesting a larger number of lower luminosity galaxies at higher redshifts.

Bouwens et al. (2010) detailed several observations of galaxies at $z \sim 7$–8 and summarized the evolution of the luminosity function of galaxies. From their fig. 15, we are able to extract the slope of the GSMF as a function of redshift to incorporate into our code. Using a spline fit and cubic interpolation, we are able to approximate the behaviour of α_G both at the data point as well as maximum and minimum values from the error bars provided, which range from about $-1 > \alpha_G > -2$ in the range $z \sim 0$–10 (Fig. 3). We consider only values above $\alpha_G = -2$ as the metallicity relation is undefined at the value $\alpha_G + 2 = 0$, which affects the minimum error bar approximation. For that case, we assume α_G is constant with the value of the lowest data point (-1.99) out at higher redshifts. Above $z = 8$, we again assume all values of α_G are constant. As shown in Fig. 3, the evolution of α_G implies a faster cosmic metallicity

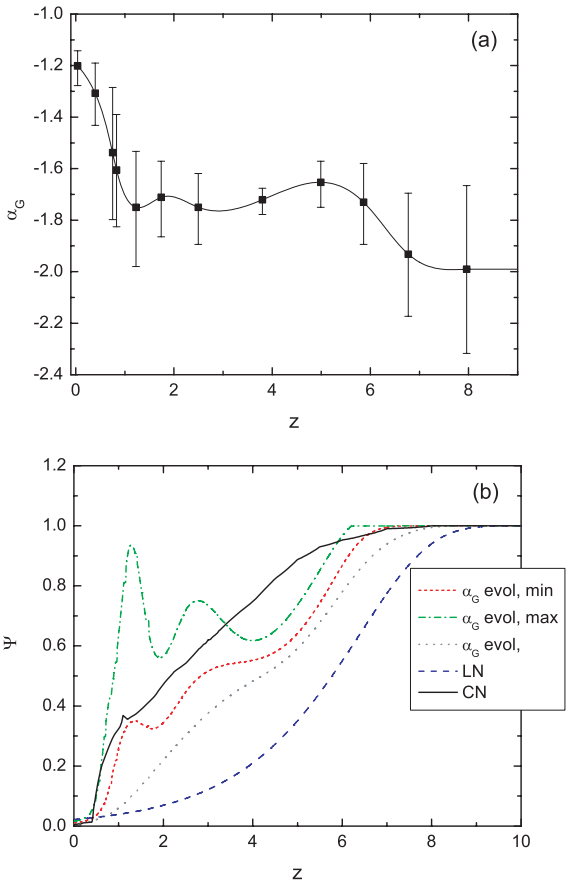

Figure 3. Panel (a): redshift evolution of the GSMF faint-end slope, α_G, including error bars (Bouwens et al. 2010). Panel (b:) effect of the evolution of α_G on the expression from LN. The $Z/Z_\odot = 0.1$ cut expression from LN and CN are included for comparison.

enrichment than just applying the unaltered expression and pushes the curve towards lower redshift and closer to the results from cosmological simulations. Using the values of the upper error bars of Fig. 3(a) gives solutions that are similar to the weighted expression of LN (Table 3).

This more realistic approach show some consistency with observation, but only in a few cases. The HB model utilizing the upper limits of the evolution of α_G and a metal cut of $Z/Z_\odot = 0.1$ shows some consistency with the L and z constraints and consistency with all $\log N$–$\log P$ constraints, while models with metallicity weighting show results only in the 3σ contour. All other HB models show little consistency in all tests, while the BL model shows some areas in the L and z constraints but shows a large deviation in the $\log N$–$\log P$ results for both BATSE and Burst Alert Telescope (BAT). The lack of consistency that is evident in most models is generally attributed to an overproduction of bursts at $z \sim 1$–2. Models utilizing the original framework of LN may show more consistency with the observations, but these set of updates are a promising and necessary direction for study that, with further enhancements, might be able to fully explain the rate increase.

4.5 GRB rate $\propto$ SFH $\times(1+z)^\delta$

As detailed in the literature (Kistler et al. 2008, 2009; Qin et al. 2010), we also consider an increase in GRB rate as $(1+z)^\delta$, where $\delta = 0.2, 0.5, 0.8$. We consider all of the SFH models with and without

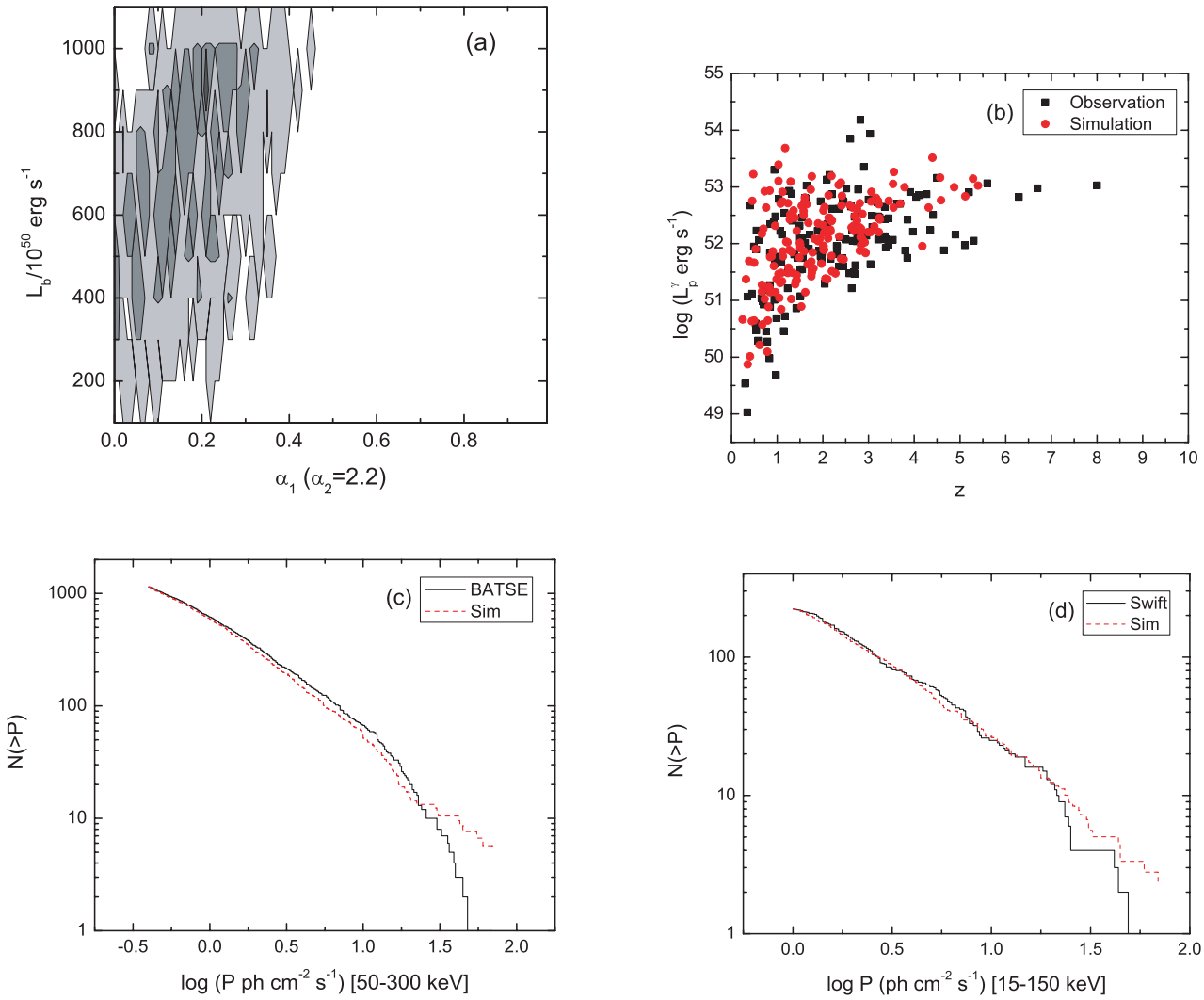

Figure 4. HB SFH model with the weighted LN expression. Panel (a): contours for consistency in both L and z. Dark grey = 2σ contour and light grey 3σ contour. Panel (b): sample 2D distribution from area of consistency in 2σ region, $(\alpha_1, \alpha_2, L_b) = (0.15, 2.2, 8 \times 10^{52}\,\mathrm{erg\,s^{-1}})$. Panels (c) and (d): BATSE and *Swift* $\log N$–$\log P$ for same parameters as panel (b).

metallicity enhancements (no GSMF evolution) and find that a few of these models are able to pass the L and z constraints but fail to pass the BATSE and *Swift* $\log N$–$\log P$ constraints (Table 4).

4.6 Luminosity function break evolution $\propto (1+z)^{\gamma}$

Lastly, we consider the evolution of the luminosity function break as detailed above. We see some consistency with the CN model and evolution with $\gamma \sim 0.5$–1.5. The 3σ regions for the CN models show areas of consistency, with a few showing 2σ significance (i.e. $\gamma =$ 1.0, 1.3) (Fig. 5). The general trend is again for shallow luminosity function slopes, the best models occurring in the area of $(\alpha_1, \alpha_2, L_b, \gamma) = (0.5, 2.2, 3 \times 10^{52}\,\mathrm{erg\,s^{-1}}, 1.0)$. The HB models show some consistency to 3σ in the same regions, although not as broadly as the CN model (Table 4).

5 SUMMARY AND DISCUSSION

Our work supports the idea that the GRB rate is enhanced at higher redshift (Daigne et al. 2006; Guetta & Piran 2007; Le & Dermer 2007; Salvaterra & Chincarini 2007; Kistler et al. 2008, 2009; Li 2008; Salvaterra 2009b,a; Qin et al. 2010; Wanderman & Piran 2010). The form of this increase, however, is still unclear. We have tested various SFH models and enhancements to the GRB rate, reflecting possible effects from changing cosmic metallicity and other evolutionary effects, with a Monte Carlo code. The resulting output was then tested for consistency with a variety of available *Swift* and BATSE data, including the L, z and peak photon flux distributions. Even when considering a numerical simulation model that takes into account a variety of realistic galactic evolution effects, both with and without metal cuts, and a metallicity relation based on the GSMF (LN), our models do not show strong consistency with the observed sample, although we believe this is the right direction for this type of study. This may indicate that metallicity is not solely responsible for the increased rate and that perhaps some other type of enhancement is needed. To this end, we test both GRB rate evolution and luminosity function (break luminosity) evolution with redshift, finding that the latter is allowed within the constraints of the BATSE and *Swift* data with moderate $[\propto L_b \times (1+z)^{\sim 0.8-1.2}]$ evolution. This statement has, of course, a few caveats. Embedded in the metallicity relation are a variety of assumptions about the GSMF and the observed mass–metallicity relation. Laskar, Berger & Chary

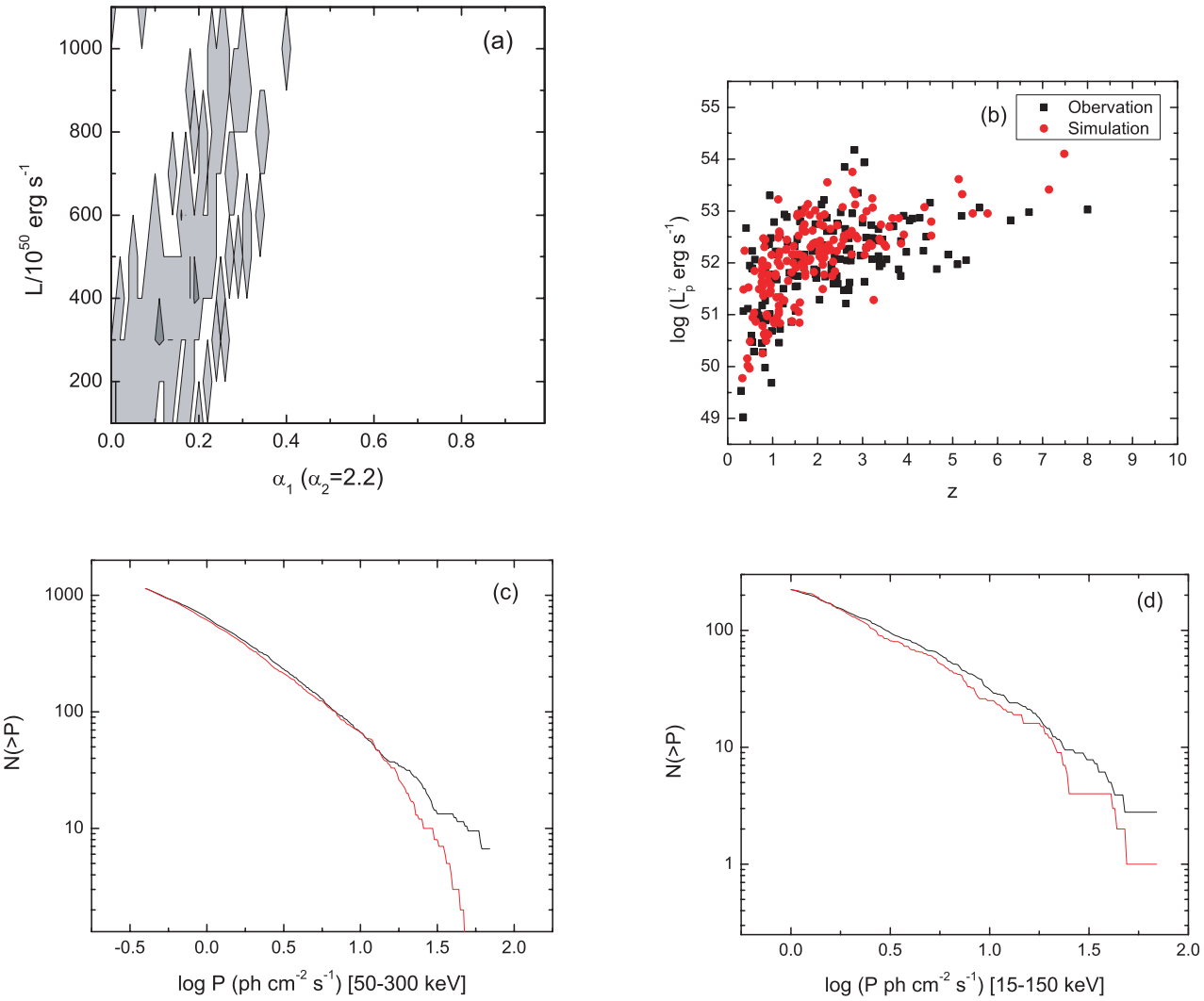

Figure 5. CN SFH model with luminosity break evolution $\propto (1+z)^{1.0}$. Panel (a): contours for consistency in both L and z. Dark grey $= 2\sigma$ contour and light grey 3σ contour. Panel (b): sample 2D distribution from area of consistency in 2σ region, $(\alpha_1, \alpha_2, L_b, \gamma) = (0.05, 2.2, 3 \times 10^{52}\,\mathrm{erg\,s^{-1}}, 1.0)$. Panels (c) and (d): BATSE and *Swift* $\log N$–$\log P$ for same parameters as panel (b).

(2011) show, using *Hubble Space Telescope* (*HST*) observations of GRB host galaxies, that the metallicity relationship likely evolves between redshifts of 3–5, which would further affect the results. It is possible that other combinations of parameters or assumptions might yield a more realistic relation, and we suggest further work on how the GSMF and stellar IMF work in tandem to affect the problem at hand. In addition, recent works have studied the M–Z relation of type II GRBs and found that the hosts lie below the Sloan Digital sky Survey (SDSS) M–Z relation (Campisi et al. 2011; Kocevski & West 2011; Mannucci, Salvaterra & Campisi 2011). This adds further evidence to the fact that the assumption of this relation for these types of bursts is likely not valid, and perhaps a consequence of the active SF environment instead of a strict metallicity cut. We have explored some basic changes, such as the evolution of the GSMF faint-end slope, but a comprehensive study of this relation or a realistic alternative are needed.

We have detailed a numerical and statistical approach aimed at understanding the properties of the GRB rate in the context of the cosmic SFH, including the constraints from newly discovered high-z bursts and the possible effects of metallicity and various types of evolution. Recent works have addressed this problem in similar (Qin et al. 2010) and fully analytical (Wanderman & Piran 2010) ways, and share some common points, although both call on fairly strong evolution of the GRB rate [$(1+z)^{\delta} \sim 0.6$–2] which we do not find. Our work also benefits from the inclusion of a fully numerical SFH model (CN) as well as a probing of the metallicity relation and cosmological considerations that may affect the GRB rate which are not included in contemporary works on the subject. Butler et al. (2010) do not find evidence of strong luminosity function or GRB rate evolution and find that a smoothed metallicity cut of $Z/Z_{\odot} = 0.2$–0.5, following the metallicity considerations of LN, can account for the observations of the current *Swift* sample, although they acknowledge that there are large errors bars. They also do not include evolution of the GSMF, which may account for the differences with this work. In addition, we analyse most components separately, and it is possible that the observed distribution is a superposition of a variety of effects. With enough computational time, the various combinations of effects can and should be tested.

By fitting the redshift distribution and $\log N$–$\log P$ distribution of BATSE and *Swift* bursts, Campisi et al. (2010) have reached the similar conclusion that type II GRBs are unbiased tracers of the SFH. Their analysis supports two possible scenarios: (i) a model

with no metal cuts and a strongly evolving luminosity function or (ii) a non-evolving luminosity function with a metal cut of $Z/Z_{\odot} < 0.3$. Both scenarios assume and fit a Schechter luminosity function. This results are similar to the results presented here, although the luminosity evolution is stronger for the non-metal cut case and the authors claim such large changes in GRB properties with redshift as unrealistic, favouring a model with a metal cut and no luminosity function evolution.

ACKNOWLEDGMENTS

This work is supported by NSF through grant AST-0908362 and by NASA through grants NNX10AD48G and NNX10AP53G. KN is supported in part by the NSF grant AST-0807491, NASA grant HST-AR-12143-01-A, National Aeronautics and Space Administration under Grant/Cooperative Agreement no. NNX08AE57A issued by the Nevada NASA EPSCoR programme, and the President's Infrastructure Award from UNLV. This research is also supported by the NSF through the TeraGrid resources provided by the Texas Advanced Computing Center.

REFERENCES

Abdo A. A. et al., 2009, Sci, 323, 1688
Abel T., Bryan G. L., Norman M. L., 2002, Sci, 295, 92
Amati L. et al., 2002, A&A, 390, 81
Band D. L., 2006, ApJ, 644, 378
Band D. et al., 1993, ApJ, 413, 281
Blain A. W., Natarajan P., 2000, MNRAS, 312, L35
Bouwens R. J. et al., 2010, preprint (arXiv:1006.4360)
Bromm V., Loeb A., 2002, ApJ, 575, 111
Bromm V., Loeb A., 2006, ApJ, 642, 382 (BL)
Butler N. et al., 2010, ApJ, 711, 495
Campisi M. A., Li L.-X., Jakobsson P., 2010, MNRAS, 407, 1972
Campisi M. A., Tapparello C., Salvaterra R., Mannucci F., Colpi M., 2011, MNRAS, preprint (arXiv:1105.1378)
Chapman R. et al., 2007, MNRAS, 382, 21
Chen H.-W., Prochaska J. X., Bloom J. S., Thompson I. B., 2005, ApJ, 634, L25
Choi J.-H., Nagamine K., 2009, MNRAS, 393, 1595
Choi J.-H., Nagamine K., 2010, MNRAS, 407, 1464 (CN)
Choi J.-H., Nagamine K., 2011a, MNRAS, 410, 2579
Choi J.-H., Nagamine K., 2011b, preprint (arXiv:1101.5656)
Cobb B. E. et al., 2006, ApJ, 645, L113
Conselice C. J. et al., 2005, ApJ, 633, 29
Coward D. M., 2005, MNRAS, 360, 77
Cusumano G. et al., 2006, Nat, 440, 164
Dai X. Y., 2009, ApJ, 697, 68
Daigne F., Rossi E., Mochkovitch R., 2006, MNRAS, 372, 1034
Davé R., Hernquist L., Katz N., Weinberg D. H., 1999, ApJ, 511, 521
Fiore F., Guetta D., Piranomonte S., D'Elia V., Antonelli L. A., 2007, A&A, 470, 515
Frail D. A. et al., 2006, ApJ, 646, L99
Fynbo J. P. U. et al., 2003, A&A, 406, L63
Gehrels N. et al., 2004, ApJ, 611, 1005
Gorosabel J. et al., 2005, A&A, 444, 711
Greiner J. et al., 2009, ApJ, 693, 1610
Guetta D., Piran T., 2007, J. Cosmol. Astropart. Phys., 7, 3
Guetta D., Piran T., Waxman E., 2005, ApJ, 619, 412
Haardt F., Madau P., 1996, ApJ, 461, 20
Haislip J. B. et al., 2006, Nat, 440, 181
Hjorth J. et al., 2003, Nat, 423, 847
Holland S. T. et al., 2010, ApJ, 717, 223
Hopkins A. M., Beacom J. F., 2006, ApJ, 651, 142 (HB)
Jakobsson P., Malesani D., Hjorth J., Fynbo J. P. U., Milvang-Jensen B., 2011, Astron. Nachr., 332, 276
Kann D. A. et al., 2011, ApJ, 734, 96
Katz N., Weinberg D. H., Hernquist L., 1996, ApJS, 105, 19
Kawai N. et al., 2006, Nat, 440, 183
Kennicutt R. C., 1998, ARA&A, 36, 189
Kistler M. D., Yüksel H., Beacom J. F., Stanek K. Z., 2008, ApJ, 673, 119
Kistler M. D., Yüksel H., Beacom J. F., Hopkins A. M., Wyithe J., Stuart B., 2009, ApJ, 705, 104
Kocevski D., West A. A., 2011, ApJ, 735, L8
Komatsu E. et al., 2011, ApJS, 192, 18
Lamb D. Q., Reichart D. E., 2000, ApJ, 536, 1
Langer N., Norman C. A., 2006, ApJ, 638, L66 (LN)
Laredo T. J., Wasserman I. M., 1998, ApJ, 502, 75
Laskar T., Berger E., Chary R.-R., 2011, preprint (arXiv:1102.1019)
Le T., Dermer C. D., 2007, ApJ, 661, 394
Levesque E., Kewley L. J., Graham J. F., Fruchter A. S., 2010, ApJ, 712, 26
Li L. X., 2008, MNRAS, 388, 1487
Liang E.-W., Dai Z. G., 2004, ApJ, 606, L29
Liang E. W., Zhang B., Virgili F., Dai Z. G., 2007, ApJ, 662, 1111
Lloyd-Ronning N. M., Fryer C., Ramirez-Ruiz E., 2002, ApJ, 574, 554
Lloyd-Ronning N. M., Dai X., Zhang B., 2004, ApJ, 601, 371
Mannucci F., Salvaterra R., Campisi M. A., 2011, MNRAS, 414, 1263
Metzger M. R., Djorgovski S. G., Kulkarni S. R., Steidel C. C., Adelberger K. L., Frail D. A., Costa E., Frontera F., 1997, Nat, 387, 878
Niino Y., Choi J.-H., Masakazu A. R., Nagamine K., Totani T., Zhang B., 2011, ApJ, 726, 88
Norris J. P., 2002, ApJ, 579, 386
Pian E. et al., 2006, Nat, 442, 1011
Porciani C., Madau P., 2001, ApJ, 548, 522 (PM)
Qin S. F., Liang E. W., Lu R. J., Wei J. Y., Zhang S. N., 2010, MNRAS, 406, 558
Sakamoto T. et al., 2007, ApJ, 669, 1115
Salvaterra R., Chincarini G., 2007, ApJ, 656, L49
Salvaterra R. et al., 2009a, MNRAS, 396, 299
Salvaterra R. et al., 2009b, Nat, 461, 1258
Savaglio S. et al., 2005, ApJ, 635, 260
Schaye J. et al., 2010, MNRAS, 402, 1536
Schmidt M., 2001, ApJ, 552, 36
Scholz F. W., Stephens M. A., 1987, J. Amer. Stat. Assoc., 82, 918
Soderberg A. M. et al., 2006, Nat, 442, 1014
Springel V., 2005, MNRAS, 364, 1105
Springel V., Hernquist L., 2003, MNRAS, 339, 289
Stanek K. Z. et al., 2003, ApJ, 591, L17
Starling R. L. C. et al., 2005, A&A, 442, L21
Stern B. E., Atteia J.-L., Hurley K., 2002, ApJ, 578, 304
Tanvir N. et al., 2009, Nat, 461, 1254
Totani T., 1999, ApJ, 511, 41
Tremonti C. A. et al., 2004, ApJ, 613, 898
van Paradijs J. et al., 1997, Nat, 386, 686
Virgili F. J., Liang E.-W., Zhang B., 2009, MNRAS, 392, 91
Virgili F. J., Zhang B., O'Brien P. T., Troja E., 2011, ApJ, 727, 109
Wanderman D., Piran T., 2010, MNRAS, 406, 1944
Wang F. Y., Dai Z. G., 2011, ApJ, 727, 34
Wijers R. A. M. et al., 1998, MNRAS, 294, L13
Zhang B. et al., 2009, ApJ, 703, 1696
Zhang B.-B. et al., 2011, ApJ, 730, 141

This paper has been typeset from a TEX/LATEX file prepared by the author.